Physics of Plasmas ARTICLE pubs.aip.org/aip/pop

Thermal Weibel instability induced magnetic fields co-exist with linear wakes in laser-ionized plasmas

Cite as: Phys. Plasmas **31**, 072108 (2024); doi: 10.1063/5.0207697
Submitted: 10 March 2024 · Accepted: 24 June 2024 ·
Published Online: 16 July 2024

Yipeng Wu,[1,2,a)] Audrey Farrell,[1] Mitchell Sinclair,[1] Chaojie Zhang,[1] Irina Petrushina,[3] Navid Vafaei-Najafabadi,[3] Marcus Babzien,[4] William Li,[4] Igor Pogorelsky,[4] Mikhail Polyanskiy,[4] Mikhail Fedurin,[4] Karl Kusche,[4] Mark Palmer,[4] Kenneth A. Marsh,[1] and Chan Joshi[1]

AFFILIATIONS

[1]Electrical and Computer Engineering Department, University of California Los Angeles, Los Angeles, California 90095, USA
[2]Tsung-Dao Lee Institute & School of Physics and Astronomy, Shanghai Jiao Tong University, Shanghai 201210, China
[3]Department of Physics and Astronomy, Stony Brook University, Stony Brook, New York 11794, USA
[4]Accelerator Test Facility, Brookhaven National Laboratory, Upton, New York 11973, USA

[a)]**Author to whom correspondence should be addressed:** yipeng.wu@sjtu.edu.cn

ABSTRACT

When a moderately intense, few-picosecond-long laser pulse ionizes gas to produce an underdense plasma column, a linear relativistic plasma wave or wake can be excited by the self-modulation instability that may prove useful for multi-bunch acceleration of externally injected electrons or positrons to high energies in a short distance. At the same time, due to the anisotropic temperature distributions of the ionized plasma electrons, the Weibel instability can self-generate magnetic fields throughout such a plasma on a few picoseconds timescale that can persist even longer than the lifetime of the wake. In the present paper, we first show using simulations that both these effects do indeed co-exist in space and time in the plasma. Using our simulations, we make preliminary estimates of the contribution to the transverse emittance growth of an externally injected beam due to the Weibel magnetic fields in a few-millimeter-long plasma. We then present the results of an experiment that has allowed us to measure the spatiotemporal evolution of the magnetic fields using an ultrashort relativistic electron probe beam. Both the topology and the lifetime of the Weibel instability induced magnetic fields in the experiment are in reasonable agreement with the fields induced by the Weibel instability in the simulations.

I. INTRODUCTION

A wake is a disturbance trailing behind but attached to a piston or a driver as it propagates through a fluid.[1] A high-intensity ($a_0 > 2$) short ($\tau < \pi c/\omega_p$) laser pulse or a high-density ($n_b > n_p$), high-energy ($\gamma \gg 1$), and tightly focused (σ_r and $\sigma_z < c/\omega_p$) charged particle bunch can excite a relativistic wake ($v_{ph} \sim c$) in an ionized gas—in a process known as laser wakefield acceleration (LWFA) or plasma wakefield acceleration (PWFA), respectively.[2–4] Here, a_0 is the normalized vector potential of the laser pulse, τ is the pulse duration, n_p is the plasma density, c/ω_p is the plasma skin depth, γ is the relativistic Lorentz factor corresponding to the phase velocity of the wake v_{ph}, n_b is the peak density of the charged particle bunch, and σ_r and σ_z are the rms bunch length and radius. Highly nonlinear (plasma density modulation $n_1/n_p \geq 1$), plasma wakes are considered for ultrahigh-gradient electron acceleration,[5–9] betatron x-ray radiation generation,[10,11] delivering electrons for radiotherapy,[12] and producing high-brightness beams for compact free electron lasers.[13–15] At the other extreme, a longer and modest-intensity laser pulse ($a_0 < 1$) or a medium-current ($I_{peak} <$ a few kiloamperes) electron bunch propagating through a preformed plasma can excite a linear plasma wave [$n_1/n_p \sim O(0.1)$] via the self-modulation instability. Here, the laser pulse, or the electron bunch, is typically one to a few picoseconds long. The main attraction of a linear wake is that it can be used to accelerate positrons or electrons injected into a single or multiple wave buckets. This is possible because such linear relativistic wakes can oscillate coherently in plasmas long after the driver has passed (typically for tens of picoseconds). Therefore, it behooves us to investigate if there are other physical processes resulting from the self-organization of the plasma that may interfere with the acceleration of particles by the wake. An example of one such effect is the generation of long-wavelength magnetic field structures[16,17] that can grow and saturate in the plasma on this timescale. If the magnetic field has a field component transverse to the velocity of the charged particle being accelerated by the wake, the particles will be deflected via the $\boldsymbol{v} \times \boldsymbol{B}$ force, leading to an increase in the transverse emittance (area occupied by the particles in transverse phase space) of the accelerated beam. Although wakefield generation by the self-modulation instability has been studied experimentally by various diagnostic techniques,[18–23] the self-generated magnetic fields in a finite radius (bounded by the slowly expanding sheath) plasma have not been hitherto observed, mainly because a suitable experimental technique to measure these fields did not exist until recently.[24]

In this paper, we first use three-dimensional (3D) particle-in-cell (PIC) simulations to show that a moderately intense laser pulse $[a_0 \leq O(1)]$ can ionize a gas to produce a plasma, generate a wake (via the self-modulation instability), and produce magnetic fields (via the so-called thermal Weibel instability[16,17]). We then show the results of an experiment that has allowed us to unambiguously measure the spatiotemporal evolution of the magnetic fields in such a plasma generated by a picosecond CO_2 laser pulse with high spatiotemporal resolution. This was achieved by imaging the deflections of an external relativistic electron probe beam that transversely propagates and overlaps with the wake. We found that these fields grow and saturate on a timescale of several picoseconds and persist for tens of picoseconds. They can, therefore, co-exist in time and space with the wake. We also find that the topology, magnitude, and evolution of these fields are consistent with the thermal Weibel instability expected in a transversely bounded plasma. Wakefield generation is a nonlinear effect ($\propto \nabla E^2$), whereas the generation of magnetic fields in the plasma is an example of self-organization of plasma currents arising from kinetic effects.[24] Our PIC simulations confirm that these two physically different phenomena can and do spatially and temporally co-exist.

Here, we consider the self-modulated LWFA[25–27] rather than the normal LWFA because the shortest pulse duration that can currently be achieved for a CO_2 laser (wavelength $\sim 9.2\ \mu$m) is ~ 2 ps (FWHM). The reason for using a CO_2 laser is that for a relatively low-density plasma one can generate a relativistic wake necessary for the acceleration of externally injected modest-energy charged particles to high energies (tens to hundreds of million electron volts) in a relatively short (few millimeter) distance. For the simulation shown in this paper, the plasma density is $n_p = 1 \times 10^{17} \mathrm{cm}^{-3}$, which gives wavelength of a relativistic wake to be $2\pi c/\omega_p = 105.5\ \mu$m, far shorter than the $\sim 750\ \mu$m (FWHM) pulse width of the laser pulse. When the pulse length of the laser is many wake periods long, the self-modulation instability can both modulate the laser pulse at the plasma period and excite a plasma wake. We, therefore, first briefly discuss the physics behind the self-modulation instability and the thermal Weibel instability.

The self-modulation instability[25–27] is a multi-dimensional instability that reduces to the forward Raman scattering instability[28] in a one-dimensional (1D) case when the laser spot size is larger than the plasma wake wavelength. If the plasma density is homogeneous over this spatial scale, the instability grows from either the plasma noise (e.g., collective Thomson scattering from longitudinal density fluctuations in the plasma) or intensity fluctuations that are present in all real laser pulses. In the exact forward direction, the forward Raman scattering instability produces both frequency up (anti-Stokes)- and down (Stokes)-shifted scattered photons that travel in the same direction as the incident photons because of phase matching. Interference of the incident and the scattered photons reinforces the density fluctuations and thus scatters more light. This causes the plasma wave and the scattered light waves to grow exponentially in the forward direction as in a classic four-wave parametric instability.[28] In the case of self-modulation instability, the noise fluctuations in the plasma density or on the laser pulse alternately focus and defocus the incident laser, causing the amplitude modulation of the laser envelope to grow as the laser pulse propagates in the plasma. Both these instabilities produce Stokes and anti-Stokes sidebands to the laser frequency each separated from the next sideband by the plasma frequency. In the special case where the plasma is long compared with the laser pulse length, the forward Raman instability is a spatiotemporal instability—that is to say, that the growth rate of the instability depends not only on laser pulse duration but also on how far the laser pulse has propagated into the plasma.[29]

Depending on the plasma density, the laser pulse can also undergo relativistic self-guiding if the laser power P exceeds the critical power for self-focusing ($P > P_{cr}$), where $P_{cr}\,(\mathrm{GW}) = 17.4 n_c/n_p$, and $n_c = 1.32 \times 10^{19}\ \mathrm{cm}^{-3}$ is the critical plasma density for a $9.2\ \mu$m-wavelength laser).[30] In the paper by Esarey *et al.*[26] the authors asserted that relativistic self-focusing was critical to the self-modulation instability. They stated that P/P_{cr} needed to be larger than roughly 1/2 (depending on the sharpness of the rise time) in order for strong self-modulation instability to occur. However, in a later work,[27] it was shown that for any given value of plasma density, a pulse length can be chosen such that the self-modulation (or forward Raman scattering) instability can still occur within a Rayleigh length Z_r. As we will see, the formation of a linear wake does not need the laser pulse to be relativistic as long as the lengths of the pulse and the plasma are sufficiently long so that the instability can grow from noise by several e-foldings.

There are many similarities between a wake generated by a single short but intense laser pulse and that generated by self-modulation of a longer intense laser pulse. In both cases the wake is relativistic, and in the linear regime, it has a longitudinal electric field E_z that scales as $\sqrt{n_e}$ V/cm. This E_z field has a sinusoidal form, making it suitable for accelerating both electrons and positrons. Electrons can be accelerated in the region where E_z is negative, whereas the positrons can be accelerated in the positive field region. However, the longitudinal field has a variation in the transverse direction which makes extraction of the energy from the wake (by beam loading) while keeping a very narrow energy spread very challenging. It requires precise beam shaping in all three dimensions. One way is to make the wake one dimensional (radius $\gg 2\pi\, c/\omega_p$), while keeping the accelerating beam very narrow. However, in this case, the energy extraction from the wake can be rather inefficient. A second option is to split the electron or positron bunch into many microbunches that are separated by $\sim 2\pi c/\omega_p$. This concept of acceleration of tens of microbunches contained within a single macrobunch has been demonstrated in a warm prototype of an S/X-band conventional accelerator.[31,32] In principle, a similar technique could be employed in a plasma accelerator to increase the total charge that can be accelerated and to improve the wake-to-macrobunch energy extraction efficiency, as long as no other mechanisms can generate large electric or magnetic fields in the plasma that would reduce the brightness of the accelerated electron bunchlets by increasing their transverse emittance.

So what process can lead to the spontaneous generation of large-scale [O(c/ω_p)] electric or magnetic fields on a timescale (few $1/\omega_p$) that would interfere with the particles that are being accelerated in the multi-bunch scenario described above? It turns out that if the rising edge of the drive laser pulse itself is used to produce the plasma, then kinetic effects—namely, the Weibel and the current filamentation instabilities arising from the anisotropic/nonthermal electron velocity distribution (EVD) functions—can give rise to macroscopic magnetic fields through self-organization of electron currents that originate from the spatial noise present in the temperature anisotropy. Such kinetic instabilities have been extensively studied by plasma theorists,[33] but only recently have we realized how to produce a nonthermal plasma with a highly controlled degree of electron temperature anisotropy to induce such instabilities. While plasma electrons can be nonthermal and hot, plasma ions remain essentially cold.[34] The process that generates such nonequilibrium plasmas is the underlying ionization mechanism, which can be single photon ionization (photon energy $h\nu > I_p$), multiphoton ionization (MPI, $nh\nu > I_p$), or tunneling ionization.[34] Here, I_p is the ionization potential of the atom. Unlike single photon ionization, MPI and tunneling ionization are strong field effects. MPI dominates when the total energy of a few photons exceeds the ionization potential, whereas tunneling ionization dominates when the electron can tunnel through the potential barrier of the atom suppressed by the laser field (in far less time than half a laser cycle). MPI is the dominant mechanism in the high-frequency photon limit, while tunneling is important in the long-wavelength laser limit.[35] In all cases, the ionized electron is emitted in the direction of the laser electric field. However, as we will show in Sec. II, in the case of tunneling ionization, the newly ionized electron can have a very large drift energy depending on the phase of the laser field at which it tunnels through the potential barrier and becomes free.[24] While understanding if high-field ionization physics has given rise to attosecond science,[36] its impact on plasma physics has only now been recognized.[36] Tunnel-ionized plasmas are dominated by kinetic effects until electron–electron collisions first thermalize the electrons, and electron–ion collisions subsequently equalize the electron and ion temperatures, which at these densities can take tens of picoseconds.[37]

II. 3D PIC SIMULATIONS

Now we show a 3D PIC simulation using the code OSIRIS[38] that illustrates how both the self-modulation and the Weibel instabilities can evolve together in a plasma. Although OSIRIS can include both ion motion and electron–ion and electron–electron collisions, we do not include these effects here to isolate the collisionless (kinetic) effects. This simulation mimics the experimental conditions of the experiment (described later in this paper) carried out at Brookhaven National Laboratory's Accelerator Test Facility (BNL-ATF). The plasma is formed by ionizing hydrogen gas emanating from a supersonic gas jet using a linearly polarized [45° from the horizonal (x–z) plane] CO_2 laser pulse that propagates in the z direction. To see the evolutions of both the self-modulation instability generated wake and the thermal Weibel instability induced magnetic fields, the simulation used a large stationary window with dimensions of $2000 \times 480 \times 480(c/\omega_0)^3 \approx 2928 \times 703 \times 703\,(\mu\mathrm{m})^3$ in the z, x, and y directions, respectively, where $\omega_0 = 2\pi c/\lambda_0$ is the CO_2 laser frequency with $\lambda_0 = 9.2\,\mu$m the wavelength. Atomic hydrogen gas was initialized inside the simulation box with atomic density linearly rising from zero at $z = 0$ to $n_p = 1 \times 10^{17}\,\mathrm{cm}^{-3}$ at $z = 1$ mm followed by a 1.6 mm long density plateau, after which the density quickly drops to zero. In the other two orthogonal directions, the gas density is uniform. We note that in order to save the computation cost, the simulation box only covers the beginning 2.6 mm region of the ~6 mm long plasma (~4 mm long density plateau with ~1 mm long density ramps on each side) in the actual experiment, which is also the region that is probed for the magnetic fields in the experiment. The CO_2 laser has a FWHM pulse duration of ~2 ps, a focal spot size of $W_0 \approx 100\,\mu$m, and an energy of ~0.2 J, leading to a peak intensity of $\sim 6 \times 10^{14}\,\mathrm{W/cm^2}$ and a normalized vector potential of $a_0 \approx 0.2$. The vacuum focal plane of the CO_2 laser is set to $z = 3$ mm. The laser pulse duration is sufficiently long for the laser to dissociate the hydrogen gas followed by ionization of the atomic hydrogen. Therefore, in the simulations, the ionization of atomic hydrogen is calculated using the Ammosov–Delone–Krainov (ADK) model.[39] The plasma electrons are sampled by 16 macro-particles per cell and the ions are assumed to be immobile.

A. Anisotropic plasma temperatures

The phase space evolution of the ionized electrons at 2.8 ps and 35.8 ps after the passage of the peak of the laser pulse in the center of the simulation box (defined as time zero) is shown in Figs. 1(a) and 1(b). The corresponding EVD evolution at both times is also plotted in Figs. 1(a) and 1(b). By fitting a Gaussian function to the EVD, we can obtain the evolution of plasma temperatures in the three dimensions $T_{e||}$, $T_{e\perp}$, and T_{ez} [see Fig. 1(c)], where the subscripts || and $\perp$ denote the directions parallel and perpendicular to the laser polarization direction in the x–y plane, respectively. As clearly shown, the plasma electrons at $t = 2.8$ ps are hot in the laser polarization direction but cold in the other two orthogonal directions. Also given are the temperature anisotropy factors $A_{||\perp} = T_{e||}/T_{e\perp} - 1$ and $A_{||z} = T_{e||}/T_{ez} - 1$ [see Fig. 1(d)]. At $t = 2.8$ ps, the plasma is highly anisotropic with temperature anisotropy factors $A_{||\perp}$ and $A_{||z} > 10$. Thereafter $A_{||\perp}$ and $A_{||z}$ keep dropping due to the isotropization of the plasma driven by kinetic instabilities.[40]

B. Evolution of the plasma wake

Figures 2(a) and 2(b) show the plasma density n_e and the longitudinal electric field E_z at three different times, 13.8, 24.8, and 35.8 ps, respectively. The most striking feature is that the plasma density n_e is bounded by a sheath that separates it from the surrounding neutral gas. The width (transverse size) of the plasma is ~300 μm, which is relatively narrow (just a few plasma wavelengths). The sheaths have a large transverse electric field (E_y ~100 MV/m) but they are extremely localized, and electrons that have energies less than the sheath potential are reflected by the sheath electric field. Also one can see from Fig. 2(b) that there is a quasi-sinusoidal plasma wake as a result of the self-modulation instability of the CO_2 laser pulse. The wake is harder to discern in the electron density plot. At the earliest time shown here ($t = 13.8$ ps), the laser pulse has already left the box. The wavelength of this wake, ~105.5 μm, is equal to that of a relativistic plasma wave $2\pi c/\omega_p$ indicating that we are exciting a linear wake [see the black dashed lines in Fig. 2(b)]. Even at $t = 35.8$ ps, the wavelength remains roughly the same, indicating that there is little phase mixing of the electron trajectories and the wake remains quasi-sinusoidal. This long coherent structure is promising for accelerating both electron and

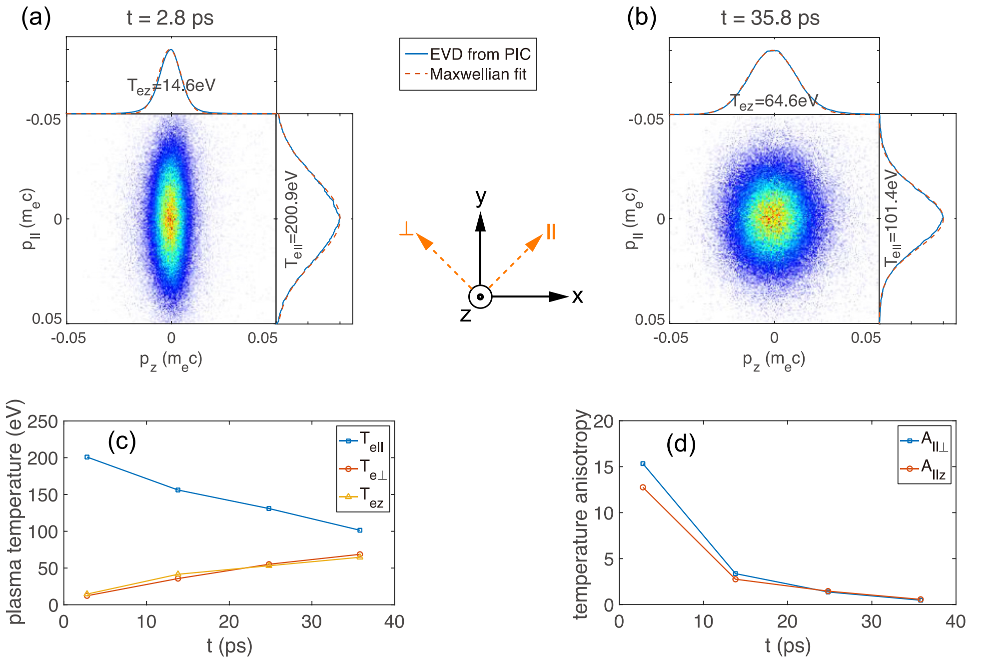

FIG. 1. (a) and (b) show the phase space as well as the EVD distributions of the plasma electrons from $z = 1.85$ to $z = 2.15$ mm at $t = 2.8$ and $t = 35.8$ ps, respectively. The evolutions of the temperature and anisotropy of the plasma electrons are shown in (c) and (d), respectively.

positron microbunches, but this will be addressed elsewhere. Although the amplitude of E_z later decays, its initial value of $\sim$200 MV/m agrees with the theoretical prediction of linear wake ($\sim a_0^2 E_p/2$, where E_p is the wave breaking limit of the cold plasma).

C. Evolution of the Weibel magnetic fields

In addition to the electric fields of the linear plasma wake driven by the self-modulation instability, magnetic fields are expected to be simultaneously generated via the thermal Weibel instability. We

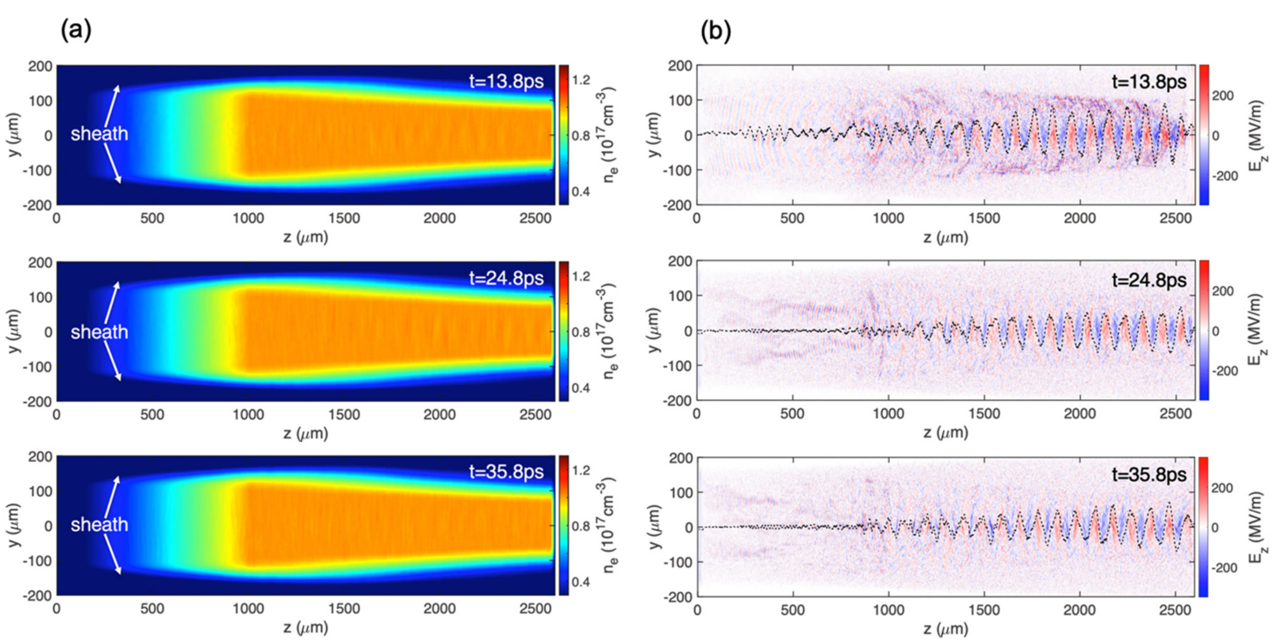

FIG. 2. The plasma density n_e (a) and the longitudinal electric field E_z (b) in the y–z plane ($x = 0$) at $t = 13.8$ ps (top row), $t = 24.8$ ps (middle row), and $t = 35.8$ ps (bottom row), respectively. The laser pulse propagates from the left to the right. The black dashed line in each frame of (b) shows the corresponding smoothed central lineout of E_z at $y = 0$. Note that the density modulation is weak in (a), but the plasma wake can be seen more clearly in the electric field plots shown in (b). The short-wavelength wake feature in the upramp is expected from the wake recurrence phenomenon observed in a density upramp in Ref. 41.

characterize the instability as being thermal because it arises from the temperature anisotropy (temperatures differ in different spatial directions) as originally envisioned by Weibel.[16] Despite being one of the earliest kinetic instabilities to have been anticipated, it had not been conclusively observed in a laboratory plasma because of the difficulty of initializing the plasma with a known temperature anisotropy as postulated by Weibel. A major breakthrough occurred when high-field ionization was shown to generate nearly 100% ionization of a particular bound electron in just a few laser cycles. Such plasmas were shown to be extremely nonthermal and anisotropic. Furthermore, the degree of anisotropy could be controlled by controlling the laser wavelength, polarization, charge state, etc.[24] The instability isotropizes the plasma electrons, and in the process, a small fraction of the energy is converted to magnetic fields. It should be mentioned that collisions play little or no role in the thermalization. For instance, at a relatively rarified density ($1 \times 10^{17}\,\mathrm{cm}^{-3}$) used in the simulations, the asymptotic electron temperature of the plasma electrons is $\sim$100 eV, as shown in Fig. 1(c). At this temperature, the collision time[42] [O($\sim$ns)] is much longer than 35.8 ps, the time at which the last frame in Fig. 2(b) is shown. Clearly, the rapid decrease in the anisotropy parameters $A_{||\perp}$ and $A_{||z}$, as shown in Fig. 1(d), is due to kinetic, collisionless processes.

Figure 3(a) shows the transverse magnetic fields B_y at different times. One can clearly see that B_y is transversely bounded by the plasma sheath, and in all frames it has a quasi-1D periodic distribution along the z direction, although it is initially somewhat irregular. This means that a quasi-single mode of the magnetic field has already formed in the top frame, $t = 13.8$ ps, and such a mode can maintain its topology for rest of the simulation. This is different from the evolution of Weibel magnetic fields in a wide (plasma width much larger than the plasma wavelength) plasma, where the initial morphology of the magnetic field is a 2D fish-net structure.[43] In a wide anisotropic plasma, the counter-propagating microscopic currents repel each other whereas the co-propagating microscopic currents attract each other. This coalescence of the currents keeps amplifying the magnetic field.

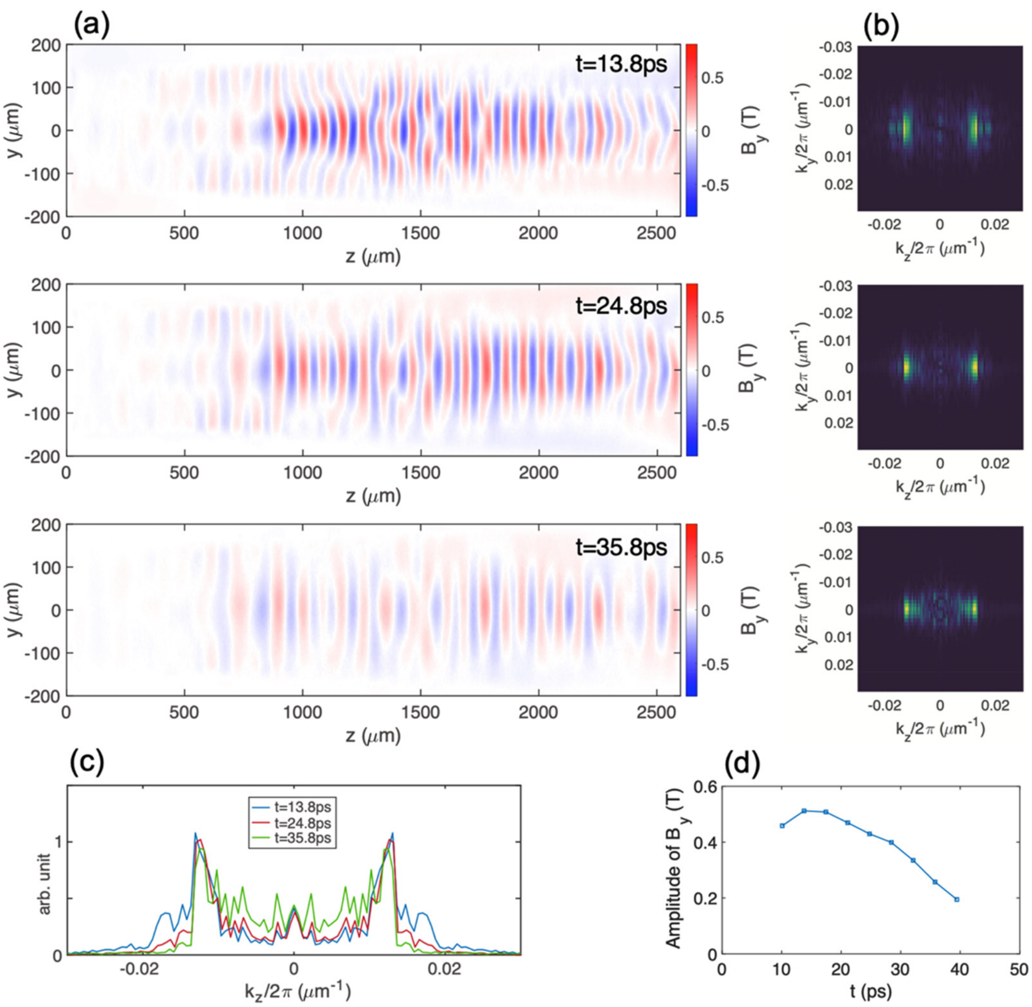

FIG. 3. The transverse magnetic field B_y (a) in the y–z plane ($x = 0$) and the corresponding 2D k-spectrum (b) obtained by taking the 2D Fourier transform of B_y at $t = 13.8$ ps (top row), $t = 24.8$ ps (middle row), and $t = 35.8$ ps (bottom row), respectively. (c) The integrated k_z-spectrum corresponding to (b). (d) The evolution of the amplitude of B_y.

Eventually current filaments are formed primarily in the cold-temperature directions (two orthogonal directions (⊥ and z) perpendicular to the laser polarization direction) and the magnetic fields also have wave vectors distributed in those directions, forming a 2D fish-net structure. However, in a bounded plasma, since the plasma is limited in size in the transverse (⊥) direction, instability modes with wavevectors along this direction and wavelengths larger than the plasma width cannot grow. Therefore, the most unstable growing mode is one with a wavevector in the longitudinal (z) direction, resulting in a quasi-1D periodic distribution of magnetic fields. We also note that the plasma currents keep merging as the instability grows and thus the spacing between the current filaments slightly increases, leading to an increase in wavelength of the magnetic fields as a function of time [see Fig. 3(a)]. This is confirmed by the k-spectra obtained by Fourier transforming the magnetic fields B_y in space, where $|k_z|$ shifts toward a smaller value [see Figs. 3(b) and 3(c)]. In addition, as shown in Fig. 3(d), the amplitude of B_y first increases as the instability grows and then reaches saturation to ∼0.5 T. After that, B_y decays with time.

In the simulations, we have probed the thermal Weibel magnetic fields and created synthetic images by mimicking the electron radiography technique that we employ in the experiment. The probing is done by sending an ultrashort (1 ps) relativistic (50.5 MeV) electron beam through the plasma at various times and recording the deflections of the electrons by the magnetic fields. In our case, if an electron probe with an initially homogeneous charge distribution is sent through the plasma along the $+x$ direction, the electrons will be mainly deflected by the magnetic field components B_y and B_z. The B_y field will cause deflections in the z direction and the B_z field will produce deflections in the y direction. These deflections then form density structures after propagating in vacuum for an optimum distance. This probing configuration is insensitive to deflections by the oscillating electric fields of the plasma wake because these fields oscillate at the plasma frequency $\omega_{\mathbf{p}}$, and as the picosecond-long probe travels through the plasma, the contributions of the wake are averaged over many periods ($\omega_{\rm p}^{-1} = 53$ fs), thus approaching zero.[44] Figure 4 shows the modulated density profiles of the electron beam at a plane located 6 mm after the plasma at different time delays, from which we can obtain the evolution of the topology and strength (amplitude) of the magnetic fields. The vertical density strips are consistent with the quasi-1D periodic structure of the magnetic field B_y along the z direction (see Fig. 4). The spacing between the density strips slightly increases with time, indicating a reduction in the wavevector (k_z) value of the magnetic field. The modulation magnitude of the density strips also increases with time and saturates at $t \approx 23.8$ ps, after which it begins to decrease. We note that the density distribution of the electron probe, apart from exhibiting a vertical stripe pattern along the z direction, is not symmetric in the y direction. The region with negative y-values has a higher electron density compared to the region with positive y-values (as indicated by the red box in Fig. 4). We find that this is mainly caused by the longitudinal component B_z of the Weibel magnetic fields.

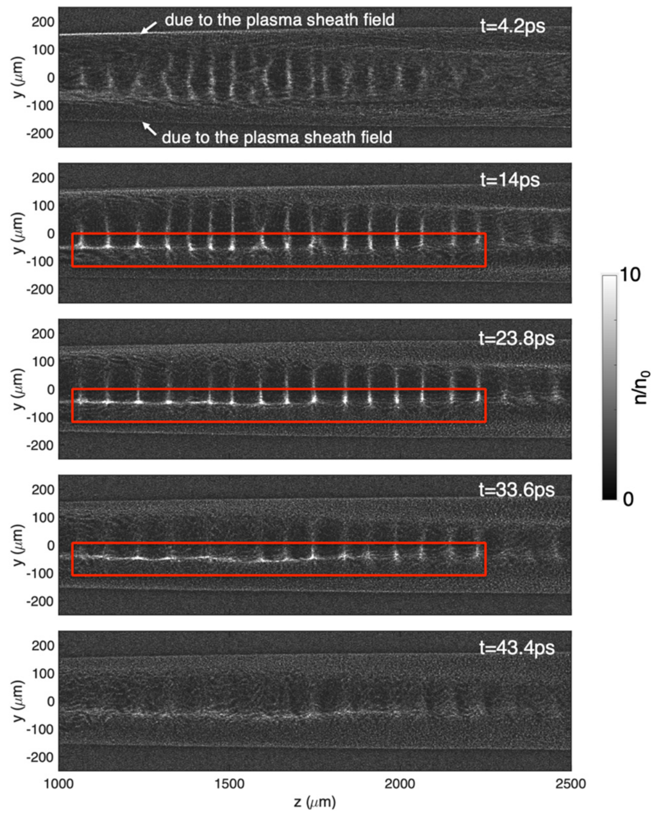

FIG. 4. Synthetic probe image at five different time delays. Note that in the synthetic image the electron beam is modulated by the transverse electric field E_y of the plasma sheaths and by both the transverse (B_y) and longitudinal (B_z) components of the Weibel magnetic fields. The Weibel magnetic fields are contained within the plasma sheath field. The red box indicates that the region with negative y-values has a higher electron density compared to the region with positive y-values.

III. EXPERIMENTS

We have carried out experiments at BNL-ATF to measure the magnetic fields induced by the Weibel instability in a laser-plasma configuration that is also expected to generate a linear wake via the self-modulation instability as discussed in Sec. II. The experimental layout is shown in Fig. 5. Plasmas with anisotropic temperatures are generated by ionizing hydrogen gas emanating from a 6-mm-long supersonic gas jet using a 2-ps, linearly polarized (45°), high-energy (∼1 J) CO_2 laser pulse.[45] Ultrashort (∼1 ps) relativistic (50.5 MeV) electron bunches produced by the ATF linear accelerator are used to probe the magnetic fields. The detailed parameters of the CO_2 laser, plasma, and electron probe beam are approximately equal to those used in the above-mentioned simulations. To achieve a high spatial resolution, a set of permanent magnet quadrupoles (PMQs[46,47]) are utilized to relay and magnify the electron probe to a YAG:Ce scintillator screen, which can convert the modulated electron flux to an optical image. The PMQ set consists of four pieces (two identical pairs) of Halbach-type high-gradient quadrupoles. These two pairs of quadrupoles were individually mounted, enabling the adjustment of their separation to modify magnification and shift the object plane location (see Fig. 5). Both assemblies were mounted on a third motorized translation stage, providing the capability to move the PMQs away from the path of the electron beam. When the movable PMQs are inserted, the object plane is positioned approximately 50 ± 0.5 mm downstream from the plasma and the image is magnified by a factor of 3.7 (further magnified by the optical system to an overall magnification of ∼17.8) with a resolution of 3.3 μm.

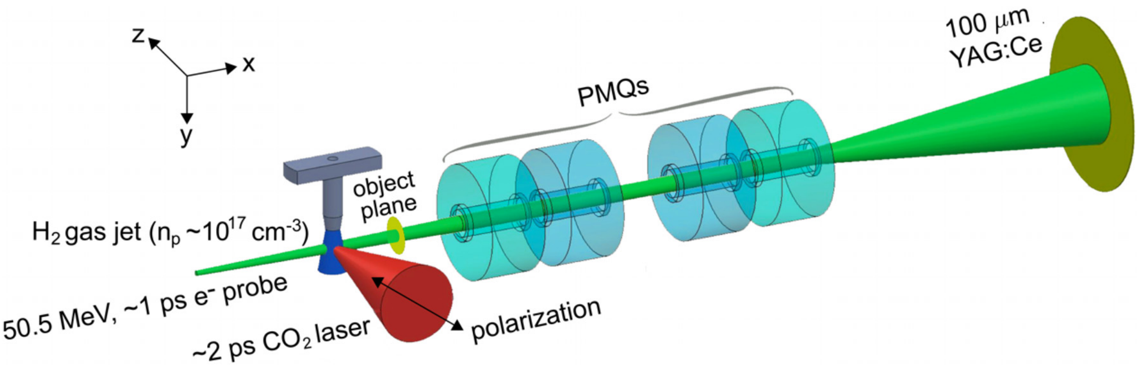

FIG. 5. Sketch of the experimental setup.

We note that we also used a $\sim$70 fs (FWHM) 800 nm laser pulse to obtain shadowgraphs of the plasma wake. However, this proved challenging due to the plasma induced refraction of the laser probe beam. By increasing the plasma density, Stokes and anti-Stokes sidebands in the CO_2 laser's spectrum became directly observable in the exact forward direction. In addition, evidence of the plasma wake emerged as sidebands at the plasma frequency in the collective Thomson scattering signal of the probe laser. Nevertheless, as the plasma density increased, the laser power approached the relativistic self-focusing threshold, leading to the rapid formation of a channel as plasma electrons were expelled. However, there are other experiments conducted at powers below the relativistic self-focusing threshold and at intensities low enough that show long lived linear plasma wakes excited by single sub-100 fs, 800 nm laser pulse.[41,48,49] Therefore, for the rest of this paper, we will focus on the measurements of the Weibel magnetic fields.

A. Topology and temporal evolution of the Weibel magnetic fields

In the experiment, by adjusting the delay between the electron probe and the CO_2 laser, we obtained a series of images of the density modulated probe beam due to deflections by the magnetic fields in the plasma. The corresponding raw images at different time delays after plasma formation are shown in Fig. 6(a). As one can see, all the frames of electron density distribution have two horizontal (parallel to the laser propagation direction) boundaries, which are caused by the transverse sheath electric fields E_y of the plasma. Between these two boundaries are the vertical density strips, and their modulation amplitudes evolve as a function of time, indicating the evolution of the magnetic field amplitudes.

Based on the measured density distribution of the electron probe, we can retrieve the path integrals of the magnetic fields along the probe propagation direction. We first computationally retrieve the deflection angles of the probe electrons by solving an equivalent optimal transport problem (see Refs. 50 and 51 for details). This method divides the beam profile into small regions called cells, and assumes that the deflection angles should be distributed in such a way that when mapping each cell of the source profile (the unperturbed electron beam profile) to the measured target profile (the beam profile at the object plane), the total displacement of all the cells should be minimized. Then, by assuming that the plasma has a slab geometry with a thickness of 300 μm, we can use the deflection angles to calculate the transverse magnetic fields. Figure 6(b) shows the retrieved path-integrated magnetic fields, B_y, at different time delays and Fig. 6(c) shows the corresponding 2D k-spectrum of B_y. The morphology of the magnetic fields in all frames is a quasi-1D periodic distribution and the corresponding wavelength increases with time, which is consistent with the continuous decrease in $|k_z|$. These results are in good agreement with the simulation results shown in Fig. 3. On the contrary, the measured magnitude of the magnetic field B_y continuously increases with time to $\sim$0.5 T at $t = 50$ ps, which is different from the simulation prediction that it first grows to the saturation value and then begins to decay. We believe that the reason is computational. In order to limit the computation time of our simulation, the number of macro-particles per cell used is relatively small (16 macro-particles per cell), resulting in certain artificial numerical collisions that cause the magnetic field to evolve faster than it should. Since the probing time window in the experiment is short compared with the evolution period of the instability, it does not capture the decaying process of the magnetic field.

IV. EFFECT OF WEIBEL MAGNETIC FIELDS ON ACCELERATED ELECTRONS

When both the linear plasma wakefield and the transverse Weibel magnetic field exist at the same time, the Weibel magnetic field will cause the deflection of the accelerated electron beam, which may lead to the deterioration of beam quality by increasing the transverse beam emittance. This effect will be the largest at low injection energies, such as at the very first stage of acceleration, where a carefully prepared, few-million electron volt microbunched beam is injected into the linear wake.[48] To examine this, we initialize a witness electron beam that follows the CO_2 laser in the simulation. The witness beam has an energy of 10 MeV and a bi-Gaussian density profile with $\sigma_r = 10$ and $\sigma_z = 150\,\mu$m. Its initial normalized emittance is set to 0.2 mm mrad. The time delay between the CO_2 laser and the witness beam is 10 ps. The simulation results show that the beam emittance growth over the course of the simulation is $\sim 40\%$ (see Fig. 7). We note that there are numerous other effects that can also increase the beam emittance in plasma-based acceleration. In a linear plasma wake, the focusing gradient varies with the longitudinal position, and different slices of the electron beam experience different focusing gradients, leading to the growth of the projected beam emittance. Therefore, the

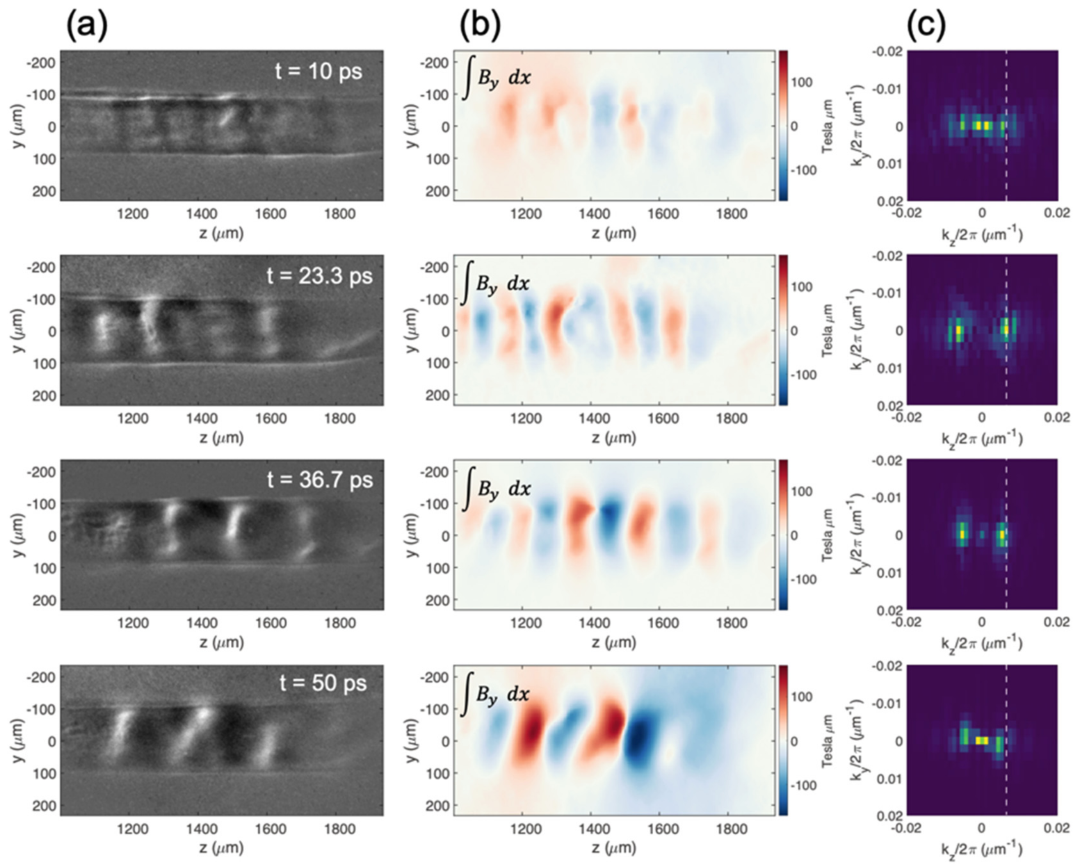

FIG. 6. Experimental results. The left column (a) shows the density modulations of the electron probe after being deflected by the magnetic fields in the plasma at different time delays. The middle (b) and right (c) columns show the corresponding retrieved $\int B_y\, dx$ and 2D k-spectrum of B_y, respectively.

emittance growth caused by the Weibel magnetic fields is even smaller than 40%. This is because the transverse magnetic field due to thermal Weibel instability is quasiperiodically distributed along the beam propagation direction, like a magnetic undulator. This magnetic field undulates the electrons with both positive and negative values, which average out the transverse beam deflections. Since the Weibel instability takes time to grow, injecting the electron beam into the plasma wake at an earlier stage would expose it to smaller amplitude magnetic fields, thereby further reducing the deleterious effect of the Weibel magnetic fields on the beam quality. However, our simulation box only covers the beginning region of the experimental plasma. The emittance growth will be larger if the witness beam propagates for a longer distance in the plasma. The full impact of these fields on accelerated beam quality requires further careful investigation.

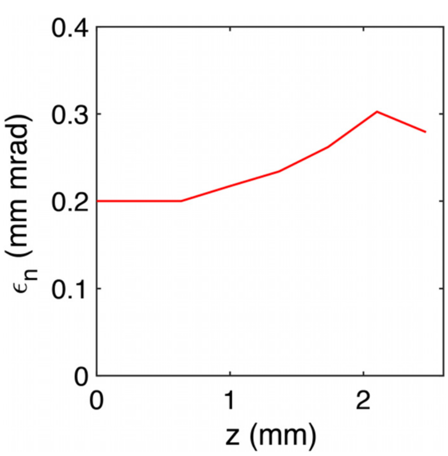

FIG. 7. Evolution of the beam normalized emittance ϵ_n.

V. SUMMARY

In summary, we have shown through self-consistent 3D PIC simulations that the thermal Weibel instability induced magnetic fields can co-exist with linear wakes in laser-ionized plasmas. We have measured the topology and the k-spectrum of the Weibel magnetic fields in an experiment using an ultrashort relativistic electron probe. The retrieved spatiotemporal evolution of the magnetic field is in good agreement with the simulation results. Our preliminary results also show that the overall deterioration of the accelerated beam quality due to thermal Weibel magnetic fields may be tolerable because the Weibel field acts as a short-wavelength quasiperiodic undulating magnetic field.

ACKNOWLEDGMENTS

We acknowledge the interest of Professor Warren B. Mori of UCLA in our work on kinetic instabilities in photoionized plasmas. We would like to acknowledge the OSIRIS Consortium, consisting of UCLA and IST (Lisbon, Portugal) for providing access to the OSIRIS 4 framework. This work was supported by DOE Grant No. DE-SC0010064:0011 and NSF Grant No. 2003354:003 at UCLA.

AUTHOR DECLARATIONS

Conflict of Interest

The authors have no conflicts to disclose.

Author Contributions

Yipeng Wu: Conceptualization (equal); Data curation (equal); Formal analysis (equal); Writing – original draft (equal); Writing – review & editing (equal). **Audrey Farrell:** Data curation (equal); Formal analysis (lead); Writing – review & editing (equal). **Mitchell Sinclair:** Data curation (equal); Writing – review & editing (equal). **Chaojie Zhang:** Formal analysis (equal); Writing – review & editing (equal). **Irina Petrushina:** Data curation (equal); Writing – review & editing (equal). **Navid Vafaei-Najafabadi:** Data curation (equal); Writing – review & editing (equal). **Marcus Babzien:** Data curation (equal); Writing – review & editing (equal). **William Li:** Data curation (equal); Writing – review & editing (equal). **Igor Pogorelsky:** Data curation (equal); Writing – review & editing (equal). **Mikhail Polyanskiy:** Data curation (equal); Writing – review & editing (equal). **Mikhail Fedurin:** Data curation (equal); Writing – review & editing (equal). **Karl Kusche:** Data curation (equal); Writing – review & editing (equal). **Mark Palmer:** Data curation (equal); Writing – review & editing (equal). **Kenneth A. Marsh:** Data curation (equal); Formal analysis (equal); Writing – review & editing (equal). **Chan Joshi:** Conceptualization (equal); Data curation (equal); Formal analysis (equal); Funding acquisition (equal); Project administration (equal); Writing – original draft (equal); Writing – review & editing (equal).

DATA AVAILABILITY

The data that support the findings of this study are available from the corresponding author upon reasonable request.

REFERENCES

[1]C. Joshi, "New ways to smash particles," Sci. Am. **325**(1), 54–61 (2021).

[2]T. Tajima and J. M. Dawson, "Laser electron accelerator," Phys. Rev. Lett. **43**, 267–270 (1979).

[3]E. Esarey, C. B. Schroeder, and W. P. Leemans, "Physics of laser-driven plasma-based electron accelerators," Rev. Mod. Phys. **81**, 1229–1285 (2009).

[4]P. Chen, J. M. Dawson, R. W. Huff, and T. Katsouleas, "Acceleration of electrons by the interaction of a bunched electron beam with a plasma," Phys. Rev. Lett. **54**, 693–696 (1985).

[5]J. Faure, Y. Glinec, A. Pukhov, S. Kiselev, S. Gordienko, E. Lefebvre, J.-P. Rousseau, F. Burgy, and V. Malka, "A laser–plasma accelerator producing monoenergetic electron beams," Nature **431**, 541–544 (2004).

[6]C. G. R. Geddes, C. Toth, J. van Tilborg, E. Esarey, C. B. Schroeder, D. Bruhwiler, C. Nieter, J. Cary, and W. P. Leemans, "High-quality electron beams from a laser wakefield accelerator using plasma-channel guiding," Nature **431**, 538–541 (2004).

[7]S. P. D. Mangles, C. D. Murphy, Z. Najmudin, A. G. R. Thomas, J. L. Collier, A. E. Dangor, E. J. Divall, P. S. Foster, J. G. Gallacher, C. J. Hooker *et al.*, "Monoenergetic beams of relativistic electrons from intense laser–plasma interactions," Nature **431**, 535–538 (2004).

[8]I. Blumenfeld, C. E. Clayton, F.-J. Decker, M. J. Hogan, C. Huang, R. Ischebeck, R. Iverson, C. Joshi, T. Katsouleas, N. Kirby *et al.*, "Energy doubling of 42 GeV electrons in a metre-scale plasma wakefield accelerator," Nature **445**, 741–744 (2007).

[9]M. Litos, E. Adli, W. An, C. I. Clarke, C. E. Clayton, S. Corde, J. P. Delahaye, R. J. England, A. S. Fisher, J. Frederico *et al.*, "High-efficiency acceleration of an electron beam in a plasma wakefield accelerator," Nature **515**, 92–95 (2014).

[10]S. Kneip, C. McGuffey, J. L. Martins, S. F. Martins, C. Bellei, V. Chvykov, F. Dollar, R. Fonseca, C. Huntington, G. Kalintchenko *et al.*, "Bright spatially coherent synchrotron X-rays from a table-top source," Nat. Phys. **6**, 980–983 (2010).

[11]S. Corde, K. Ta Phuoc, G. Lambert, R. Fitour, V. Malka, A. Rousse, A. Beck, and E. Lefebvre, "Femtosecond x rays from laser-plasma accelerators," Rev. Mod. Phys. **85**, 1–48 (2013).

[12]J. Farr, V. Grilj, V. Malka, S. Sudharsan, and M. Schippers, "Ultra-high dose rate radiation production and delivery systems intended for FLASH," Med. Phys. **49**, 4875–4911 (2022).

[13]W. Wang, K. Feng, L. Ke, C. Yu, Y. Xu, R. Qi, Y. Chen, Z. Qin, Z. Zhang, M. Fang *et al.*, "Free-electron lasing at 27 nanometres based on a laser wakefield accelerator," Nature **595**, 516–520 (2021).

[14]R. Pompili, D. Alesini, M. P. Anania, S. Arjmand, M. Behtouei, M. Bellaveglia, A. Biagioni, B. Buonomo, F. Cardelli, M. Carpanese *et al.*, "Free-electron lasing with compact beam-driven plasma wakefield accelerator," Nature **605**, 659–662 (2022).

[15]M. Labat, J. C. Cabadağ, A. Ghaith, A. Irman, A. Berlioux, P. Berteaud, F. Blache, S. Bock, F. Bouvet, F. Briquez *et al.*, "Seeded free-electron laser driven by a compact laser plasma accelerator," Nat. Photonics **17**, 150–156 (2023).

[16]E. S. Weibel, "Spontaneously growing transverse waves in a plasma due to an anisotropic velocity distribution," Phys. Rev. Lett. **2**, 83–84 (1959).

[17]B. D. Fried, "Mechanism for instability of transverse plasma waves," Phys. Fluids **2**, 337 (1959).

[18]A. Modena, Z. Najmudin, A. E. Dangor, C. E. Clayton, K. A. Marsh, C. Joshi, V. Malka, C. B. Darrow, C. Danson, D. Neely *et al.*, "Electron acceleration from the breaking of relativistic plasma waves," Nature **377**, 606–608 (1995).

[19]C. A. Coverdale, C. B. Darrow, C. D. Decker, W. B. Mori, K.-C. Tzeng, K. A. Marsh, C. E. Clayton, and C. Joshi, "Propagation of intense subpicosecond laser pulses through underdense plasmas," Phys. Rev. Lett. **74**, 4659–4662 (1995).

[20]K. Nakajima, D. Fisher, T. Kawakubo, H. Nakanishi, A. Ogata, Y. Kato, Y. Kitagawa, R. Kodama, K. Mima, H. Shiraga *et al.*, "Observation of ultrahigh gradient electron acceleration by a self-modulated intense short laser pulse," Phys. Rev. Lett. **74**, 4428–4431 (1995).

[21]R. Zgadzaj, J. Welch, Y. Cao, L. D. Amorim, A. Cheng, A. Gaikwad, P. Iapozzutto, P. Kumar, V. N. Litvinenko, I. Petrushia *et al.*, "Plasma electron acceleration driven by a long-wave-infrared laser," Nat. Commun. **15**, 4037 (2024).

[22]F. Albert, N. Lemos, J. L. Shaw, B. B. Pollock, C. Goyon, W. Schumaker, A. M. Saunders, K. A. Marsh, A. Pak, J. E. Ralph *et al.*, "Observation of betatron x-ray radiation in a self-modulated laser wakefield accelerator driven with picosecond laser pulses," Phys. Rev. Lett. **118**, 134801 (2017).

[23]N. Lemos, F. Albert, J. L. Shaw, D. Papp, R. Polanek, P. King, A. L. Milder, K. A. Marsh, A. Pak, B. B. Pollock *et al.*, "Bremsstrahlung hard x-ray source driven by an electron beam from a self-modulated laser wakefield accelerator," Plasma Phys. Controlled Fusion **60**, 054008 (2018).

[24]C. Zhang, C. K. Huang, and C. Joshi, "Self-organization of photoionized plasmas via kinetic instabilities," Rev. Mod. Plasma Phys. **7**, 34 (2023).

[25]J. Krall, A. Ting, E. Esarey, and P. Sprangle, "Enhanced acceleration in a self-modulated-laser wake-field accelerator," Phys. Rev. E **48**, 2157–2161 (1993).

[26]E. Esarey, J. Krall, and P. Sprangle, "Envelope analysis of intense laser pulse self-modulation in plasmas," Phys. Rev. Lett. **72**, 2887–2890 (1994).

[27]V. V. Goloviznin, P. W. van Amersfoort, N. E. Andreev, and V. I. Kirsanov, "Self-resonant plasma wake-field excitation by a laser pulse with a steep leading edge for particle acceleration," Phys. Rev. E **52**, 5327–5332 (1995).

[28]W. L. Kruer, *The Physics of Laser Plasma Interactions* (Addison-Wesley, Redwood City, CA, 1988).

[29]W. B. Mori, C. D. Decker, D. E. Hinkel, and T. Katsouleas, "Raman forward scattering of short-pulse high-intensity lasers," Phys. Rev. Lett. **72**, 1482–1485 (1994).

[30] P. Sprangle, C. M. Tang, and E. Esarey, "Relativistic self-focusing of short-pulse radiation beams in plasmas," IEEE Trans. Plasma Sci. **15**, 145 (1987).

[31] S. Liu, M. Fukuda, S. Araki, N. Terunuma, J. Urakawa, K. Hirano, and N. Sasao, "Beam loading compensation for acceleration of multi-bunch electron beam train," Nucl. Instrum. Methods Phys. Res., Sect. A **584**, 1–8 (2008).

[32] R. D. Ruth, C. Adolphsen, K. Bane, R. F. Boyce, D. L. Burke, R. Callin, G. Caryotakis, R. Cassel, S. L. Clark, H. Deruyter *et al.*, "A test accelerator for the next linear collider," Report No. SLAC-PUB-6293, 1993. See https://www.slac.stanford.edu/pubs/slacpubs/6250/slac-pub-6293.pdf.

[33] M. Brambilla, *Kinetic Theory of Plasma Waves: Homogeneous Plasmas No. 96* (Oxford University Press, 1998).

[34] C.-K. Huang, *Transient Plasma Effects in Optical-Field Ionized Helium Gas* (University of California, Los Angeles, 2020).

[35] P. B. Corkum, "Plasma perspective on strong field multiphoton ionization," Phys. Rev. Lett. **71**, 1994 (1993).

[36] S.-Y. Zhong, H. Teng, and Z.-Y. Wei, "From high-order harmonic generation to attosecond pulses: A review of the Nobel Prize in Physics 2023," Physics **52**(12), 816–824 (2023).

[37] C.-K. Huang, C. J. Zhang, K. A. Marsh, C. E. Clayton, and C. Joshi, "Initializing anisotropic electron velocity distribution functions in optical-field ionized plasmas," Plasma Phys. Controlled Fusion **62**, 024011 (2020).

[38] R. A. Fonseca, L. O. Silva, F. S. Tsung, V. K. Decyk, W. Lu, C. Ren, W. B. Mori, S. Deng, S. Lee, T. Katsouleas *et al.*, "OSIRIS: A three-dimensional, fully relativistic particle in cell code for modeling plasma based accelerators," in *Computational Science—ICCS 2002, Lecture Notes in Computer Science*, edited by P. M. A. Sloot, A. G. Hoekstra, C. J. K. Tan, and J. J. Dongarra (Springer, Berlin Heidelberg, 2002), pp. 342–351.

[39] M. V. Ammosov, N. B. Delone, and V. P. Krainov, "Tunnel ionization of complex atoms and atomic ions in electromagnetic field," Sov. Phys.-JETP **64**, 138 (1986).

[40] C. Zhang, C.-K. Huang, K. A. Marsh, C. E. Clayton, W. B. Mori, and C. Joshi, "Ultrafast optical field–ionized gases—A laboratory platform for studying kinetic plasma instabilities," Sci. Adv. **5**, eaax4545 (2019).

[41] C. J. Zhang, J. F. Hua, Y. Wan, C.-H. Pai, B. Guo, J. Zhang, Y. Ma, F. Li, Y. P. Wu, H.-H. Chu *et al.*, "Femtosecond probing of plasma wakefields and observation of the plasma wake reversal using a relativistic electron bunch," Phys. Rev. Lett. **119**, 064801 (2017).

[42] J. D. Huba, *NRL Plasma Formulary* (Naval Research Laboratory, Washington, DC, 2013).

[43] C. J. Zhang, Y. P. Wu, M. Sinclair, A. Farrell, K. A. Marsh, I. Petrushina, N. V. Najafabadi, A. Gaikwad, R. Kupfer, K. Kusche *et al.*, "Mapping the self-generated magnetic fields due to thermal Weibel instability," Proc. Natl. Acad. Sci. U. S. A. **119**(50), e2211713119 (2022).

[44] C. J. Zhang, J. F. Hua, X. L. Xu, F. Li, C.-H. Pai, Y. Wan, Y. P. Wu, Y. Q. Gu, W. B. Mori, C. Joshi *et al.*, "Capturing relativistic wakefield structures in plasmas using ultrashort high-energy electrons as a probe," Sci. Rep. **6**, 29485 (2016).

[45] M. N. Polyanskiy, I. V. Pogorelsky, M. Babzien, and M. A. Palmer, "Demonstration of a 2 ps, 5 TW peak power, long-wave infrared laser based on chirped-pulse amplification with mixed-isotope CO_2 amplifiers," OSA Continuum **3**, 459 (2020).

[46] Z. Zhou, Y. Fang, H. Chen, Y. Wu, Y. Du, L. Yan, C. Tang, and W. Huang, "Demonstration of single-shot high-quality cascaded high-energy-electron radiography using compact imaging lenses based on permanent-magnet quadrupoles," Phys. Rev. Appl. **11**, 034068 (2019).

[47] Z. Zhou, Y. Fang, H. Chen, Y. Wu, Y. Du, Z. Zhang, Y. Zhao, M. Li, C. Tang, and W. Huang, "Visualizing the melting processes in ultrashort intense laser triggered gold mesh with high energy electron radiography," Matter Radiat. Extremes **4**, 065402 (2019).

[48] Y. Wu, J. Hua, Z. Zhou, J. Zhang, S. Liu, B. Peng, Y. Fang, X. Ning, Z. Nie, F. Li *et al.*, "High-throughput injection–acceleration of electron bunches from a linear accelerator to a laser wakefield accelerator," Nat. Phys. **17**, 801–806 (2021).

[49] J. Jonnerby, A. von Boetticher, J. Holloway, L. Corner, A. Picksley, A. J. Ross, R. J. Shalloo, C. Thornton, N. Bourgeois, R. Walczak *et al.*, "Measurement of the decay of laser-driven linear plasma wakefields," Phys. Rev. E **108**, 055211 (2023).

[50] C. Zhang, Y. Wu, M. Sinclair, A. Farrell, K. A. Marsh, J. Hua, I. Petrushina, N. Vafaei-Najafabadi, R. Kupfer, K. Kusche *et al.*, "Electron Weibel instability induced magnetic fields in optical-field ionized plasmas," Phys. Plasmas **29**, 062102 (2022).

[51] M. F. Kasim, L. Ceurvorst, N. Ratan, J. Sadler, N. Chen, A. Sävert, R. Trines, R. Bingham, P. N. Burrows, M. C. Kaluza *et al.*, "Quantitative shadowgraphy and proton radiography for large intensity modulations," Phys. Rev. E **95**, 023306 (2017).